
Deep Neural Networks Abstract Like Humans

Alex Gain

Department of Computer Science
The Johns Hopkins University
again1@jhu.edu

Hava Siegelmann*

School of Computer and Information Sciences
UMass Amherst
hava@cs.umass.edu

Deep neural networks (DNNs) have revolutionized AI due to their remarkable performance in pattern recognition, comprising of both memorizing complex training sets¹ and demonstrating intelligence by generalizing to previously unseen data² (test sets). The high generalization performance in DNNs has been explained by several mathematical tools, including optimization,^{3,4,5,6,7,8} information theory,^{9,10} and resilience analysis.¹¹ In humans, it is the ability to abstract concepts from examples that facilitates generalization; this paper thus researches DNN generalization from that perspective. A recent computational neuroscience study revealed a correlation between abstraction and particular neural firing patterns.¹² We express these brain patterns in a closed-form mathematical expression, termed the “Cognitive Neural Activation metric” (CNA) and apply it to DNNs. Our findings reveal parallels in the mechanism underlying abstraction in DNNs and those in the human brain. Beyond simply measuring similarity to human abstraction, the CNA is able to predict and rate how well a DNN will perform on test sets, and determines the best network architectures for a given task in a manner not possible with extant tools. These results were validated on a broad range of datasets (including ImageNet and random labeled datasets) and neural architectures.

Large-scale analyses of fMRI data, spanning twenty years and tens of thousands of studies, were recently analyzed to determine a correlation between neuronal firing patterns across the whole brain and the areas most activated during a variety of tasks having different levels of abstraction.¹² As a first step, a distance metric was employed – combining latency (fMRI) and accessibility (DTI) – that measured the connectome distance (CD), i.e. how ‘far’ each Region Of Interest (ROI) was from the brain’s inputs (sensory cortices). The Regions of Interest were binned by their CD to create a layered “connectome depth network” (CDM). All fMRI experiments were projected on the CDM, and experiments that measured the same cognitive behavior (typically about 1000) were analyzed together. Findings showed that brain activity was present at all depths of the network for each cognitive behavior. However, deep neurons (those farther from brain inputs on the CDM) showed higher activation values than shallow neurons when the brain was engaged in reasoning and other abstract behaviors. When graphed against CD, this neuronal activity showed a positive slope (see Figure 1A). In contrast, shallow neurons had higher activation values than deep neurons and neuronal activity showed a negative slope when less abstract (shorter CD) tasks were performed. Each of the recorded behaviors was identifiable by a specific geometric slope on the CDM that correlated with each behavior’s level of abstraction (determined by independent survey).

We translated these results into a mathematical expression and used it to define the CNA. CNA consists of three essential components: the abstraction level $\alpha(x)$ of the input x to a network, the slope $\beta(x)$ of the firing patterns during the computation, and the correlation between the two:

$$\text{CNA} \triangleq \rho_{\alpha,\beta} \tag{1}$$

which measures whether a low abstraction correlates with a low slope and a high abstraction correlates with a high slope. For the exact definition, see the box below.

The neuroscience result is now restated as the human brain having:

$$\rho_{\alpha,\beta} \approx 1 \tag{3}$$

*The views, opinions and/or findings expressed are those of the authors and should not be interpreted as representing the official views or policies of the Department of Defense or the U.S. Government.

Defining the CNA

For a network architecture A and dataset X with n data points, define

1. $\alpha(x)$ – the abstraction level of every datapoint $x \in X$,
2. $\beta(x)$ – the slope of neuronal activity of network A when presented with $x \in X$,
3. α, β – the vectors of length n summarizing the abstraction and slope on the whole dataset X .

The CNA is defined by the Pearson correlation between the abstraction and the slope:

$$\rho_{\alpha, \beta} = \frac{\text{cov}(\alpha, \beta)}{\sigma_{\alpha} \sigma_{\beta}} \quad (2)$$

where $\text{cov}(\alpha, \beta)$ is the sample covariance of the two vectors: $\frac{1}{n-1} \sum_i (\alpha_i - \bar{\alpha})(\beta_i - \bar{\beta})$, $\bar{\alpha}$ and $\bar{\beta}$ are the means, and σ_{α} , and σ_{β} are the sample standard deviations $\frac{1}{n-1} \sum_i (\alpha_i - \bar{\alpha})^2$ and $\frac{1}{n-1} \sum_i (\beta_i - \bar{\beta})^2$.

CNA: The mathematical expression of a neuroscience property describing how humans abstract.

where X is the set of cognitive behaviors performed by humans, the slopes $\beta(x)$ were obtained by the data analysis (Figure 1A), and the levels of abstraction $\alpha(x)$ for each cognitive task was determined via independent survey. Respondents were asked to order cognitive tasks after viewing common definitions of *abstraction* (see [12], Supplementary Material), as following:

1. A process of creating general concepts or representations ... often with the goal of compressing the information content ... and retaining only information which is relevant.
2. Process of information aggregation, refinement, combination, integration, coalescing, accumulation, amalgamation, combination of ideas.

Moving from Neuroscience to Machine Learning, we note that the training inputs to DNNs can be classified by levels of abstraction or complexity paralleling the cognitive behaviors for the brain. We quantify these levels via the computationally tractable Shannon entropy approximation (further details in Appendix). The slope of a neural network is calculated just as was done for the neuroscience result, by summing neuronal activations in each layer and applying linear regression to arrive at a slope of neuronal activity per input x . A DNN has activation distribution patterns that are similar to the brain when $\rho_{\alpha, \beta}$ approaches 1, are unrelated to the brain when $\rho_{\alpha, \beta}$ approaches 0, and show opposite patterns to those of the brain when $\rho_{\alpha, \beta}$ approaches -1. The exact value is the level of similarity. See example in Figure 1B. The CNA ignores labels and will, therefore, work equally well on supervised and unsupervised inputs in a similar way to humans.

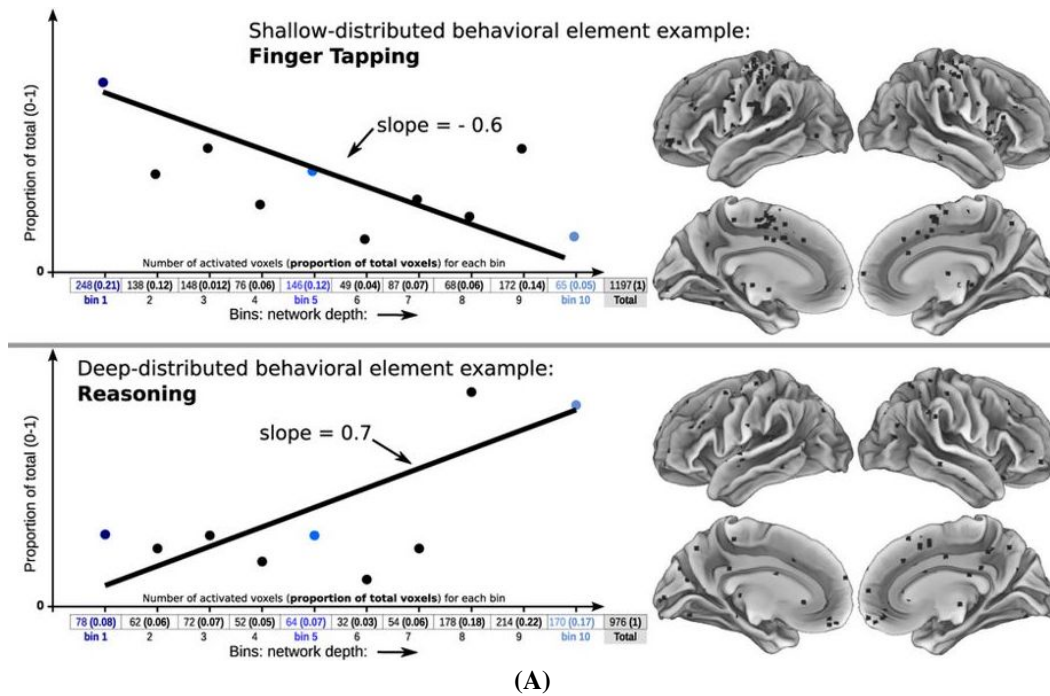
We next evaluate whether the CNA – a construct borrowed from neuroscience – can provide insight into how well a neural network will generalize to a test set. Results show that the CNA is highly correlated with test accuracy (Figure 2A). To better understand this phenomenon we demonstrate the similarity between the gradient (change in value) of the CNA and of DNN accuracy during backpropagation training (Figure 2B). See Appendix for experimental and analytical details.

Given the strong predictive power of the CNA for test accuracy, we next define a variant called the “CNA-Margin”. It has the capacity to express the difference in accuracy between the test set and the training set, often called the generalization gap. Significant differences in distributions between the training and test sets should be captured by the difference between $\alpha(X_{\text{train}})$ and $\alpha(X_{\text{test}})$, propagate to the correlated slopes $\beta(X_{\text{train}})$ and $\beta(X_{\text{test}})$, then to the difference between the two CNA values, and finally captured by the CNA-Margin (see Appendix for mathematical definitions).

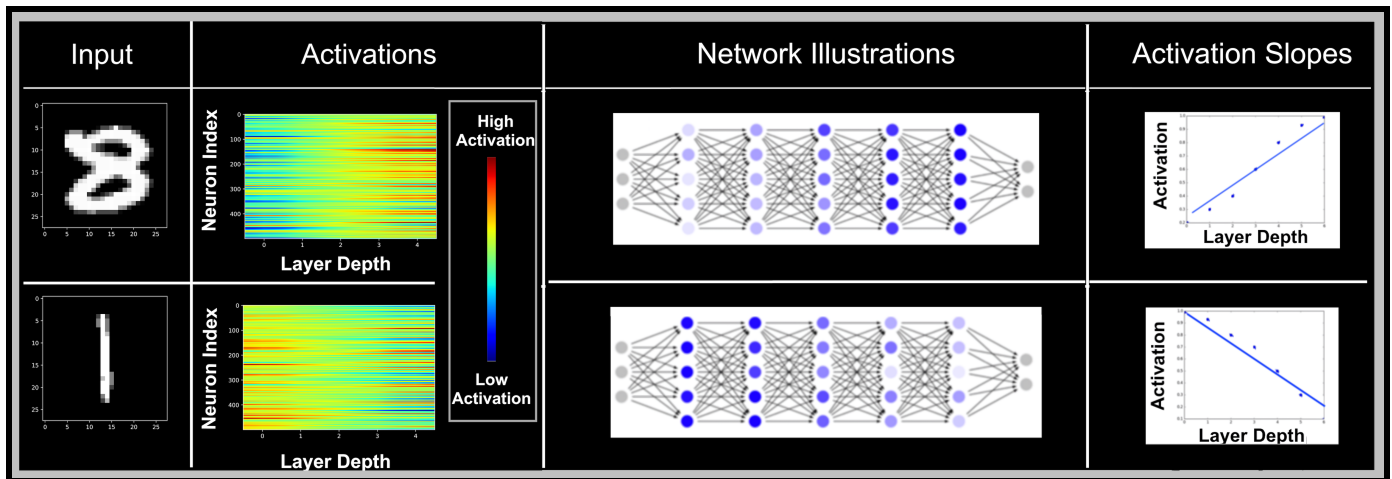
Figure 3A shows that the CNA-Margin predicts the train-test gap accuracy on the same architectures and datasets considered in Figure 2A and compares favorably to state-of-the-art generalization-gap predictors.¹³ Its strength is truly revealed when considering hard, non-standard data sets. Figure 3B repeats the experiments from 3A but also includes the Gaussian noise dataset. Each point in this

dataset is drawn from the standard normal distribution and labeled randomly to one of 10 classes. The CNA-Margin performed just as well on this hard dataset while other gap predictors failed. Similarly, the CNA-Margin shows superiority on shuffled label datasets (Figure 3C), which are equivalent to standard datasets except that subsets of training labels are randomly assigned. We considered five variations (different proportions of shuffled labels) for each of the above datasets, and no randomness in the test set, as was done in [1]. Existing measures cannot handle these datasets while the CNA can (shown in 3C). Figures 3B-C suggest that important information is found in the relationship between slope and entropy that cannot be captured through previous mathematical efforts.

Previous studies have argued that a high-level resemblance exists between DNNs and brains^{14, 15, 16, 15} and [17] measured similarity of neuronal firing between DNNs and the visual stream in the brain. However, our work is the first to borrow a neuroscientific mechanism and use it to both show that DNNs behave similarly to the human brain, and has the capacity to characterize their key property: Generalization. The CNA, serving as a common mechanism underlying abstraction in both neuroscience and deep neural networks, constitutes a practical way of analyzing abstraction and generalization in increasingly sophisticated AI.

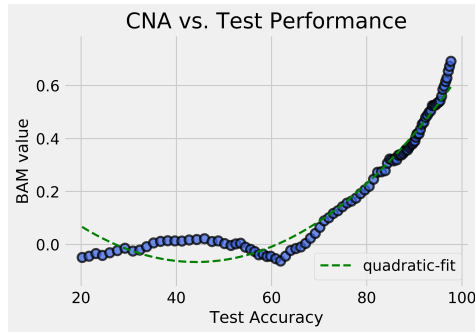


(A)

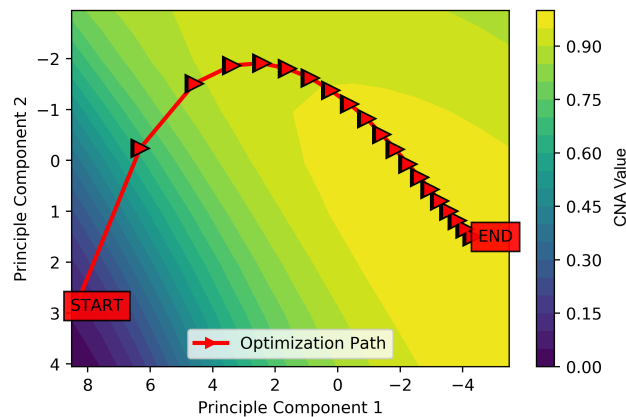


(B)

Figure 1: **Illustrations of the Cognitive Neural Activation metric (CNA).** The two subfigures show correlations between data entropy and neuronal activation pattern slope. (A) Shows firing patterns in the human brain. X-axis is the bin number, with the first bin closest to the brain's inputs and 10th bin farthest away. Y-axis is the total activation per bin, normalized over numerous experiments of the same behaviors: tapping (top) and reasoning (bottom). The geometric slope of neuronal firing correlates with the behavior's entropy (figure from [12]). (B) Plot of neuronal activations and slope of a DNN trained on MNIST. Input: digit 8 has higher entropy and digit 1 has lower entropy. Activations: x-axis corresponds to the 5 hidden layers ordered by depth; y-axis plots 500 neurons per layer; higher activations in deeper levels for digit 8, lower activations for digit 1. Network Illustrations: sketches of DNN activity (only 5 layers shown). Activation Slopes: DNN shows a positive slope when processing digit 8 and negative slope for digit 1.

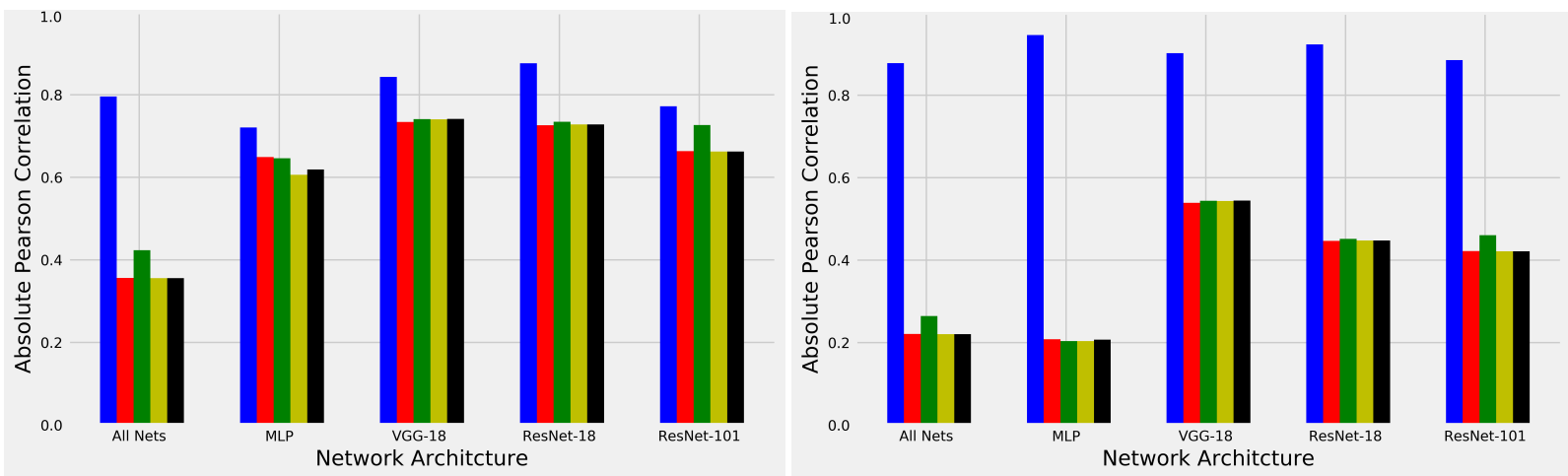


(A)



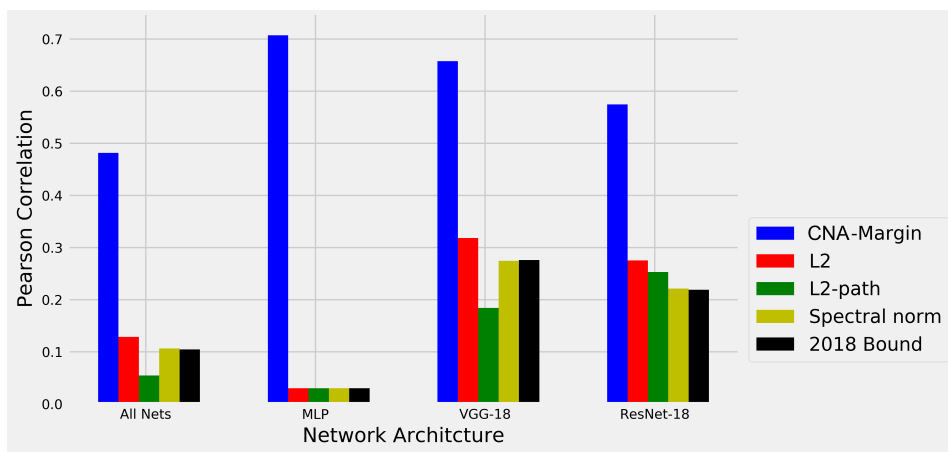
(B)

Figure 2: **The CNA strongly correlates with DNN accuracy.** (A) Test accuracy: 147 combinations across six different datasets (ImageNet, CIFAR-10, CIFAR-100, SVHN, MNIST, Fashion-MNIST), four different architectures (MLP, VGG-18, ResNet-18, and ResNet-101), and measured at multiple stages of training (every 20 passes). CNA correlates significantly with test accuracy, with a nearly linear relationship at greater than 70% suggesting neural activation properties of DNNs become more similar to the brain as classification results improve. (B) Training accuracy – illustration of a feature: During backpropagation learning, the weights change to increase accuracy, and the optimization path (visualized through PCA dimensionality reduction) concurrently leads to higher values of CNA, despite the fact that the optimization target does not include CNA. The largest rate of change occurs in early training for both the CNA and the training accuracy.



(A)

(B)



(C)

Figure 3: **The CNA is a state-of-the-art predictor of generalization in both the human brain and DNNs.** (A) The CNA-Margin predicts the gap between DNN generalization (test-set accuracy) and DNNs’ memorization capabilities (training-set accuracy) on the same 147 combinations, as in 2A: Datasets (ImageNet, CIFAR-10, CIFAR-100, SVHN, MNIST, Fashion-MNIST) and network architectures (MLP, VGG-18, ResNet-18, ResNet-100), analyzed every 20 training epochs. Superior capabilities are emphasized on the left when summarized over all network architectures. (B) CNA demonstrates further robustness when incorporating an additional non-standard dataset, the Gaussian noise dataset (see text) – for a total of 177 combinations – the original datasets (147 combinations total) plus the Gaussian noise dataset (30 combinations total). The CNA-Margin remains a robust metric, whereas other metrics break down. (C) The CNA-Margin remains comparatively robust for shuffled label datasets, with varying percentages of shuffled labels (10%, 20%, 30%, 40%, 50%) per set.

Appendix

Defining the CNA for DNNs

The CNA is the correlation between abstraction levels α and the slopes of neuronal activities β .

To define the slope β for a single datapoint, order the layers by depth (already explicitly defined for DNNs), define a method to aggregate layer-wise activation values (e.g. mean, sum, etc.), and perform a linear regression on those values to arrive at a slope.

Here we focus on input datapoints, and translate abstraction via the second definition stated in the main text, translating it to Shannon entropy.^{18,19,20,21} This is defined, for a datapoint x , as:

$$\alpha(x) \triangleq - \sum_j P(x[j]) \log P(x[j]) \quad (4)$$

where P denotes probability and $x[j]$ denotes the j -th feature of x . This is estimated through histogram binning, where values are normalized between 0 and 1, and 1000 bins are used.

We now define the CNA for a given network and batch of datapoints:

For a data point $x \in \mathbb{R}^d$ with d features, denote the entropy of x as the scalar $\alpha(x)$. We define the slope $\beta(x)$ of a given network and datapoint x . Then, we define the Cognitive Neural Activation metric $CNA_\alpha(X)$ for a given network, dataset $X \in \mathbb{R}^{n \times d}$ of size n , and entropy approximation function α .

Definition 0.1 (Slope $\beta(x)$ of Network). For a given feedforward network with L layers and input vector x , let $z_\ell^k(x)$ be the pre-activation state of neuron k in layer ℓ given input vector x , let n_ℓ be the number of neurons in layer ℓ , and let $\phi_\ell(x) = \sum_{k=1}^{n_\ell} z_\ell^k(x)$, i.e. the sum of the pre-activation values in layer ℓ . Let $\phi(x)$ be the vector of length L where $[\phi(x)]_\ell = \phi_\ell(x)$ for $\ell = 1, \dots, L$. Performing a linear regression via least squares on the points $\{(\ell, \phi_\ell(x)) \mid \ell = 1, \dots, L\}$, we obtain the slope $\beta(x)$ of the network.

Definition 0.2 (Cognitive Neural Activity $CNA_\alpha(X)$ of Network). For a given feedforward network with L layers and dataset $X \in \mathbb{R}^{n \times d}$, where n corresponds to the number of samples: Let $\alpha(X)$ be the vector of length n with entropy $\alpha(x)$ for $x \in X$ and let $\beta(X)$ be the vector of associated slopes. $CNA_\alpha(X)$ is defined as $\text{corr}(\alpha(X), \beta(X))$, where corr denotes Pearson correlation.

The sum of pre-activation values aggregation function showed consistency across many architectural choices – including Batch Normalization, Dropout, and pooling layers. Including versus not including the output layer as part of the CNA computation did not change our results, hence we included it for simplicity in our experiments.

Analytic Similarities Between the Gradients for Supervised Loss and the CNA

Consider: Databatch X consisting of n samples and corresponding label batch Y and error terms \mathcal{E} , network layers $1, \dots, L$, let n_ℓ denote the number of neurons in layer ℓ , and let z_ℓ^k denote the activation value of the network for neuron k in layer ℓ . Lastly denote the supervised loss as $C(X, Y)$. Then the supervised loss gradient² derives to:

$$\nabla C(X, Y) = \frac{1}{n} \sum_{x \in X, \varepsilon \in \mathcal{E}} \varepsilon \nabla z_L(x) \quad (5)$$

And the CNA gradient³ derives to:

$$\nabla CNA_\alpha(X) = \frac{1}{n} \sum_{x \in X} \alpha(x) \nabla \beta(x) \quad (6)$$

²For brevity, our expressions correspond to the 1-dimensional output case (derivations straightforwardly generalize to larger output dimensions).

³Also for brevity, we consider the mean-aggregated CNA gradient without the standard deviation normalization terms. The direction of the non-normalized CNA gradient is approximately equal to the direction of CNA gradient with these terms included, i.e. they have a cosine similarity of close to 1 in practice. The direction is what is important since our analysis is primarily concerned with the cosine similarity between the supervised loss and CNA gradients (cosine similarity is invariant to scaling).

The slope gradient is defined by

$$\nabla\beta(x) = \sum_{\ell=1}^L \frac{C_{\ell}^{\dagger}}{n_{\ell}} \sum_{k=1}^L \nabla z_{\ell}^k(x) \quad (7)$$

where C^{\dagger} is the row of the pseudoinverse matrix used in the least squares regression corresponding to the slope term $\beta(x)$.

Focusing on the terms ε , $\alpha(x)$, $\nabla z_L(x)$, and $\nabla\beta(x)$, we observe some resemblance between the two gradients. They both have scalars (ε and $\alpha(x)$) multiplied by gradients of network output terms ($\nabla z_L(x_i)$ and $\nabla\beta(x)$). We now show that the terms in both pairs are closely related.

On the similarity of $\nabla z_L(x)$ and $\nabla\beta(x)$: Note that $\nabla\beta(x)$ is a weighted sum⁴ of network output terms ∇z_{ℓ} for $\ell = 1, \dots, L$. There is similarity between $\nabla z_L(x)$ and $\nabla\beta(x)$ since they are both linear functions of activation output gradients. In practice, when training on the MNIST dataset with an MLP network, we find that, for the vast majority of datapoints, the cosine angle between $\nabla z_L(x)$ and $\nabla\beta(x)$, when using mean-aggregated activations, does not exceed 0.05 radians, meaning their directions are *very* similar.

Given this large degree of similarity between $\nabla z_L(x)$ and $\nabla\beta(x)$, if ε and $\alpha(x)$ correlate, we would expect updates via $\nabla C(X, Y)$ and $\nabla CNA_{\alpha}(X)$ to take the network along similar optimization paths. Experiments show this to be the case, with significant correlation, greater than 0.5, across training time.

Experimental Details

We present the experimental details for our generalization results.

For the MLP architecture, the depth was fixed at 5 hidden layers of size 500 each. Regularization was not used for the MLPs, but batch-normalization was used for the VGG-18 and ResNet architectures. Max-pooling was used after every block of the VGG-18 and ResNet architectures followed by average pooling in the last block.

For VGG and ResNet architectures, standard image augmentation was used for SVHN, CIFAR-10, CIFAR-100, and ImageNet. Otherwise, image augmentation was not used. Across all experiments, ImageNet was downsampled²² to resolution 32 x 32 for computational expediency.

Across all experiments, training continued until approximately 0 training loss was achieved. For all standard datasets, we trained MLPs for 100 epochs with a learning rate of 0.05 and momentum of 0.8 via SGD. For the VGG-18 and ResNet experiments, a learning rate of 0.01 and momentum of 0.8 were used. The VGG and ResNet architectures were trained for 100 epochs on CIFAR-10 and CIFAR-100, 40 epochs on MNIST, Fashion-MNIST, and SVHN, and 50 epochs on ImageNet. On ImageNet, the MLP architecture was excluded from analysis since it failed to converge passed 32% training accuracy after 1000 epochs. For the Gaussian noise dataset, the same optimization settings were used except all architectures were trained for 40 epochs (since this was a sufficient number for memorization of the training set).

The Gaussian noise dataset is of training size 50,000 and test size 10,000, where datapoints are of shape (3,32,32), are drawn from the standard normal distribution, and are then normalized between 0 and 1. A total of 10 classes are randomly assigned to each datapoint.

For results shown in Figure 2A, a quadratic fit of the form $ax^2 + bx + c$ was performed to arrive at the green dotted curve shown. Points were smoothed in bins of 25 networks each, ordered by test accuracy, for cleaner visualization. For Figure 2B, we used the MLP network trained on MNIST (achieving around 98% test accuracy) with the CNA value scaled between 0 and 1; for PCA visualization, network states were recorded at each training iteration.

For the shuffled label datasets (MNIST, Fashion-MNIST, SVHN, CIFAR-10, CIFAR-100), for each experiment, a percentage of the training labels was shuffled and trained on with a new network. The percentages considered were 10%, 20%, 30%, 40%, and 50%, with metrics of the network measured at the end of training once approximately 0 training error had been achieved, for a total

⁴In fact, given the nature of C^{\dagger} , it can be shown that $\nabla\beta(x)$ is a weighted *average* of ∇z_{ℓ} terms.

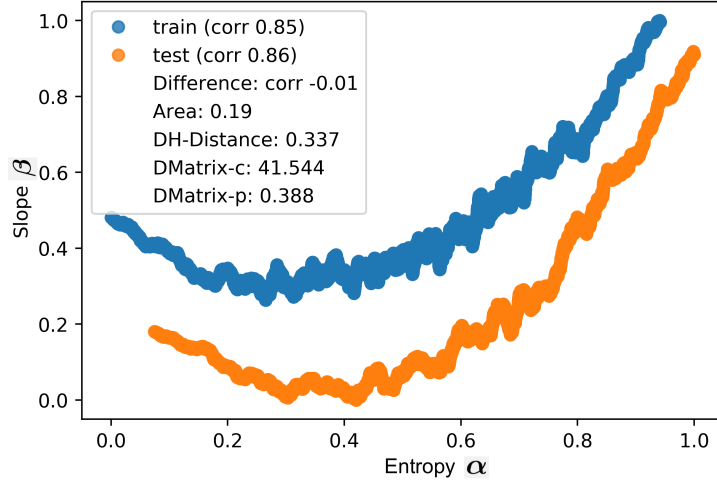


Figure 4: **Slope-Entropy Curves.** Plot of the slope-entropy values of an MLP trained on SVHN. The linearity of the curves correlates well with test performance, and the gap between the two curves correlates well with train-test loss gap.

of 75 additional trained networks considered. All training settings were consistent with the original datasets, except the number of epochs were doubled, since shuffled label datasets require more training iterations to memorize the training set.¹ In Figure 3C, the networks at the end of training on shuffled label datasets were incorporated into analysis of the networks trained every 20 epochs on the corresponding non-shuffled datasets. Lastly, for the MLP architecture, other metrics (L2, L2-path, Spectral norm, and the 2018 bound) *negatively* correlated with generalization gap, performing particularly bad in comparison to other settings, thus we show them at 0 correlation for ease of visualization. In contrast, all metrics had the same sign for Pearson correlation in 3A-B, thus absolute Pearson correlation was shown (for ease of comparison).

CNA-Margin Motivation and Definition

Recall that the CNA is defined as the Pearson correlation between the slope and entropy measure for a given dataset X , i.e. $\text{corr}(\alpha(X), \beta(X))$. For networks that perform well on their test sets, this correlation is significantly positive, indicating the relationship between $\alpha(X)$ and $\beta(X)$ is highly linear. For networks that perform poorly, the CNA is close to zero or is slightly negative. However, this says nothing about whether a network’s output distribution significantly differs between training and test instances: For example, for a CNA value of zero, no relationship between $\alpha(X)$ and $\beta(X)$ exists but, nonetheless, the loss on both the training and test set could be very similar, resulting in a small generalization gap.

Thus, it is necessary to consider the relationship between $\alpha(X)$ and $\beta(X)$ on both the training and test set. If the distribution significantly differs on the training and test sets, we would expect the distribution of $\beta(X)$ to change as well, altering the relationship.

Define the *slope-entropy curve* of a dataset X as the set of tuples

$$\{(\alpha(x), \beta(x)) \mid x \in X\} \quad (8)$$

The generalization gap would then be reflected by the difference in the slope-entropy curves of the training and test sets. This is illustrated in Figure 4 for the SVHN dataset and MLP architecture.

Quantifying this difference, we define the estimated area between the slope-entropy curves for a given training set X_{train} and test set X_{test} as the maximum area over the set of polygons that can be inscribed between the slope-entropy curves of X_{train} and X_{test} , i.e.

$$\text{CNA}_{\mathcal{A}}(X_{\text{train}}, X_{\text{test}}) \triangleq \max_{P \in \mathcal{S}} A(P) \quad (9)$$

where $A(P)$ denotes the area of a polygon P , and \mathcal{S} denotes the set of polygons that can be inscribed between the curves.

As was done for the metrics in [13], we scale $CNA_{\mathcal{A}}(X_{\text{train}}, X_{\text{test}})$ by the margin of the network. The margin, an important component in Support Vector Machines and other machine learning algorithms,²³ is defined as the minimum distance to a decision boundary²⁴ for a given network. To define this in closed-form, consider a classification setting with H classes and a network f with an output layer of size H . For a single datapoint x , the network output $f(x) \in [0, 1]^H$ is a vector of probabilities with each index $f(x)[j]$ denoting the probability, estimated by f , that x belongs to class j . The margin is defined, for a single datapoint x and network A as

$$\gamma \triangleq f(x)[j_{\text{true}}] - \max_{j \neq j_{\text{true}}} f(x)[j] \quad (10)$$

where j_{true} denotes the correct groundtruth class that x belongs to. In practice, for computational tractability, the margin of a network is taken to be the maximum γ over a set of datapoints, typically between 1% to 10% of the training datapoints, which we denote as γ_{margin} . We then arrive at our final generalization gap metric, termed the CNA-Margin, and denoted as $CNA_{\mathcal{M}}$:

$$CNA_{\mathcal{M}}(X_{\text{train}}, X_{\text{test}}) \triangleq \gamma_{\text{margin}} \cdot CNA_{\mathcal{A}}(X_{\text{train}}, X_{\text{test}}) \quad (11)$$

References

- ¹ Chiyuan Zhang, Samy Bengio, Moritz Hardt, Benjamin Recht, and Oriol Vinyals. Understanding deep learning requires rethinking generalization. *arXiv preprint arXiv:1611.03530*, 2016.
- ² Yann LeCun, Yoshua Bengio, and Geoffrey Hinton. Deep learning. *nature*, 521(7553):436, 2015.
- ³ Yann N Dauphin, Razvan Pascanu, Caglar Gulcehre, Kyunghyun Cho, Surya Ganguli, and Yoshua Bengio. Identifying and attacking the saddle point problem in high-dimensional non-convex optimization. In *Advances in neural information processing systems*, pages 2933–2941, 2014.
- ⁴ Kenji Kawaguchi. Deep learning without poor local minima. In *Advances in Neural Information Processing Systems*, pages 586–594, 2016.
- ⁵ Quynh Nguyen and Matthias Hein. The loss surface of deep and wide neural networks. *arXiv preprint arXiv:1704.08045*, 2017.
- ⁶ Anna Choromanska, Mikael Henaff, Michael Mathieu, Gérard Ben Arous, and Yann LeCun. The loss surfaces of multilayer networks. In *Artificial Intelligence and Statistics*, pages 192–204, 2015.
- ⁷ Hao Li, Zheng Xu, Gavin Taylor, and Tom Goldstein. Visualizing the loss landscape of neural nets. *arXiv preprint arXiv:1712.09913*, 2017.
- ⁸ Poorya Mianjy, Raman Arora, and Rene Vidal. On the implicit bias of dropout. *arXiv preprint arXiv:1806.09777*, 2018.
- ⁹ Naftali Tishby and Noga Zaslavsky. Deep learning and the information bottleneck principle. In *Information Theory Workshop (ITW), 2015 IEEE*, pages 1–5. IEEE, 2015.
- ¹⁰ Ravid Shwartz-Ziv and Naftali Tishby. Opening the black box of deep neural networks via information. *arXiv preprint arXiv:1703.00810*, 2017.
- ¹¹ Ari S Morcos, David GT Barrett, Neil C Rabinowitz, and Matthew Botvinick. On the importance of single directions for generalization. *arXiv preprint arXiv:1803.06959*, 2018.
- ¹² P Taylor, JN Hobbs, J Burrioni, and HT Siegelmann. The global landscape of cognition: hierarchical aggregation as an organizational principle of human cortical networks and functions. *Scientific reports*, 5:18112, 2015.
- ¹³ Behnam Neyshabur, Srinadh Bhojanapalli, David McAllester, and Nati Srebro. Exploring generalization in deep learning. In *Advances in Neural Information Processing Systems*, pages 5947–5956, 2017.
- ¹⁴ Yoshua Bengio and Asja Fischer. Early inference in energy-based models approximates back-propagation. *arXiv preprint arXiv:1510.02777*, 2015.

- ¹⁵ Benjamin Scellier and Yoshua Bengio. Equilibrium propagation: Bridging the gap between energy-based models and backpropagation. *Frontiers in computational neuroscience*, 11:24, 2017.
- ¹⁶ Yoshua Bengio, Thomas Mesnard, Asja Fischer, Saizheng Zhang, and Yuhuai Wu. Stdp-compatible approximation of backpropagation in an energy-based model. *Neural computation*, 29(3):555–577, 2017.
- ¹⁷ Martin Schrimpf, Jonas Kubilius, Ha Hong, Najib J Majaj, Rishi Rajalingham, Elias B Issa, Kohitij Kar, Pouya Bashivan, Jonathan Prescott-Roy, Kailyn Schmidt, et al. Brain-score: Which artificial neural network for object recognition is most brain-like? *BioRxiv*, page 407007, 2018.
- ¹⁸ Hamparsum Bozdogan. Akaike’s information criterion and recent developments in information complexity. *Journal of mathematical psychology*, 44(1):62–91, 2000.
- ¹⁹ David Freides. Human information processing and sensory modality: Cross-modal functions, information complexity, memory, and deficit. *Psychological bulletin*, 81(5):284, 1974.
- ²⁰ Jaume Rigau, Miquel Feixas, and Mateu Sbert. An information-theoretic framework for image complexity. In *Proceedings of the First Eurographics conference on Computational Aesthetics in Graphics, Visualization and Imaging*, pages 177–184. Eurographics Association, 2005.
- ²¹ I Mario, M Chacon, D Alma, and S Corral. Image complexity measure: a human criterion free approach. In *Fuzzy Information Processing Society, 2005. NAFIPS 2005. Annual Meeting of the North American*, pages 241–246. IEEE, 2005.
- ²² Patryk Chrabaszcz, Ilya Loshchilov, and Frank Hutter. A downsampled variant of imagenet as an alternative to the cifar datasets. *arXiv preprint arXiv:1707.08819*, 2017.
- ²³ Harris Drucker, Christopher JC Burges, Linda Kaufman, Alex J Smola, and Vladimir Vapnik. Support vector regression machines. In *Advances in neural information processing systems*, pages 155–161, 1997.
- ²⁴ Gamaleldin Elsayed, Dilip Krishnan, Hossein Mobahi, Kevin Regan, and Samy Bengio. Large margin deep networks for classification. In *Advances in Neural Information Processing Systems*, pages 842–852, 2018.
- ²⁵ Jia Deng, Wei Dong, Richard Socher, Li-Jia Li, Kai Li, and Li Fei-Fei. Imagenet: A large-scale hierarchical image database. In *2009 IEEE conference on computer vision and pattern recognition*, pages 248–255. Ieee, 2009.
- ²⁶ Alex Krizhevsky and Geoffrey Hinton. Learning multiple layers of features from tiny images. Technical report, Citeseer, 2009.
- ²⁷ Yuval Netzer, Tao Wang, Adam Coates, Alessandro Bissacco, Bo Wu, and Andrew Y Ng. Reading digits in natural images with unsupervised feature learning. 2011.
- ²⁸ Yann LeCun, Léon Bottou, Yoshua Bengio, Patrick Haffner, et al. Gradient-based learning applied to document recognition. *Proceedings of the IEEE*, 86(11):2278–2324, 1998.
- ²⁹ Han Xiao, Kashif Rasul, and Roland Vollgraf. Fashion-mnist: a novel image dataset for benchmarking machine learning algorithms. *arXiv preprint arXiv:1708.07747*, 2017.